Supplementary information

Coherent exciton dynamics in ensembles of size-dispersed CdSe quantum dot dimers probed via ultrafast spectroscopy: a quantum computational study

Hugo Gattuso[1], Barbara Fresch[2], R. D. Levine[3,4,5], F. Remacle[1*]

[1] Theoretical Physical Chemistry, Research Unit Molecular Systems, University of Liege, B4000 Liege, Belgium

[2] Department of Chemical Sciences, University of Padova, Italy

[3] The Fritz Haber Center for Molecular Dynamics and Institute of Chemistry, The Hebrew University of Jerusalem, Jerusalem 91904, Israel

[4] Department of Molecular and Medical Pharmacology, David Geffen School of Medicine and

[5] Department of Chemistry and Biochemistry, University of California, Los Angeles, CA 90095, USA

*email : fremacle@uliege.be

Table of content

1. Single particle model
2. Excitonic model for the dimer
3. Computation of the excitonic Coulomb integrals
4. Computation of the transition dipole matrix elements
5. Dispersion of the electronic properties as a function of the ensemble of dimers

1. Single particle model

The EMA and **k.p** parabolic expansion at the Γ point provide a one particle Schroedinger equation for the radial envelope functions. The one particle Schroedinger Hamiltonian for the holes and the electron is written :

$$H_i\phi_i(\mathbf{r}) = \left(-\frac{\hbar^2}{2}\nabla\frac{1}{m_i(\mathbf{r}_i)}\nabla + V_i(\mathbf{r}_i)\right)\phi_i(\mathbf{r}) = E_i\phi_i(\mathbf{r}) \qquad (1)$$

In Eq. (1), i represents a hole or an electron, the eigen function $\phi_i(\mathbf{r})$ and E_i are the wave function and the energies of the radial envelope wave function and $V_i(\mathbf{r}_i)$ is the confining spherical potential of radius a

$$V_i(r) = \begin{cases} 0 & r < a \\ V_i^0 & r > a \end{cases} \qquad (2)$$

Eq.(1) can be solved implicitly by imposing the continuity of the wave function and its first derivative on the border of the confining potential, see for example[1]. One obtains :

$$\phi_n^i(\mathbf{r}) = \frac{R_n^i(r)}{\sqrt{4\pi}} = R_n^\alpha(r) = \left[\theta(a-r)A_n\frac{\sin(k_{in}^{i,n}r)}{r} + \theta(r+a)B_n\frac{\exp(-k_{out}^{i,n}r)}{r}\right] \qquad (3)$$

with

$$k_{in}^{i,n} = \sqrt{2m_i^* E_n^i/\hbar^2} \text{ and } k_{out}^{i,n} = \sqrt{2m_i^0\left(V_0^i - E_n^i\right)/\hbar^2} \qquad (4)$$

m_i^* is the effective mass of the hole or the electron inside the dot, m_e^*=0.13 and m_h^*=0.82. m_i^0 the effective mass outside the dot and taken equal to 1. The depth of the confinement potentials depend on the dot size and were estimated from the empirical relation given in ref.[2] : $V_0^e(a) = 3.49 + 2.47(2a)^{-1.32}$, $V_0^h(a) = 5.23 + 0.74(2a)^{-0.95}$. We therefore consider three one particle levels per dot, see Figure S1.

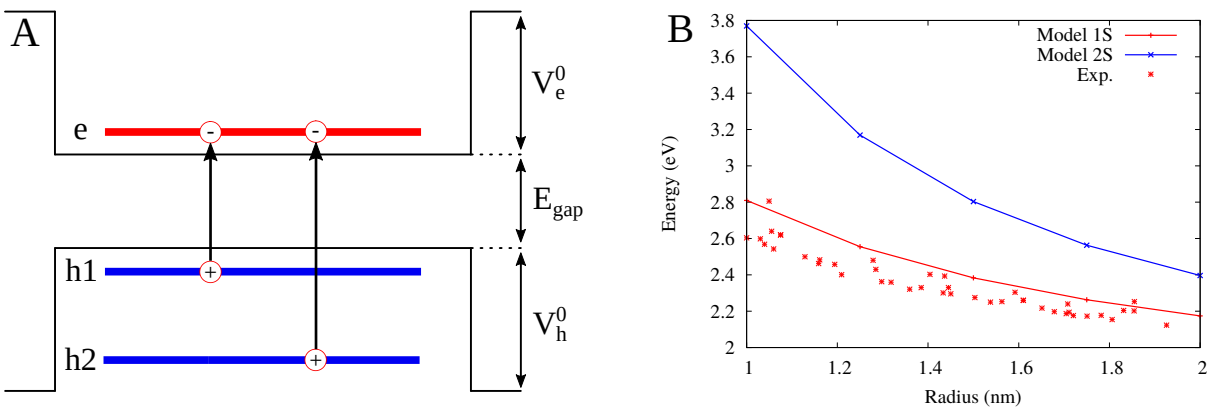

Figure S1. A. The two hole and one electron single particle states considered in the model. E_{gap} is the bulk gap value. The arrows show the two excitons that can be built from these three states. B. Comparison of the results of our model using the parameters listed above with experimental data from Refs. [2-4]

2. Excitonic model for the dimer

Once the energies and wave functions of the single particle (hole and electron) have been determined, one can build an effective two particle excitonic Hamiltonian $\hat{H}_{eh}(\mathbf{r},\mathbf{r}')$.

$$\hat{H}_{eh}(\mathbf{r},\mathbf{r}') = \hat{H}_e(\mathbf{r}) + \hat{H}_h(\mathbf{r}') + \hat{V}_{Coulomb}(|\mathbf{r}-\mathbf{r}'|) + E_{gap} \quad (5)$$

where the two one particle $\hat{H}_{e/h}(\mathbf{r})$ are given by Eq. (1) and E_{gap} is the value of the bulk band gap, see Figure S1.

The exciton basis functions are two-particle wave functions, given as the product of the hole and the electron wave function solutions of Eq. (1):

$$\phi_{ij}^{he} = \phi_i^{h*}(\mathbf{r}_1,\sigma_1)\phi_j^e(\mathbf{r}_2,\sigma_2) \quad (6)$$

where i = 1Se and j = 1Sh$_{3/2}$, 2Sh$_{3/2}$. There are two exciton states per QD, the GS exciton 1Se-1Sh$_{3/2}$ and the first excited exciton 1Se- 2Sh$_{3/2}$. In the basis of the exciton antisymmetrized singlet basis functions, the Hamiltonian (Eq. (5)) [5, 6] takes the form:

$$H_{ij,i'j'} = \left(E_i^e - E_j^h\right)\delta_{ii'}\delta_{jj'} - J_{ij,i'j'} + K_{ij,i'j'} \quad (7)$$

with the Coulomb

$$J_{ij,i'j'} = \sum_{\sigma_1\sigma_2} \iint d\mathbf{r}_1 d\mathbf{r}_2 \phi_i^h(\mathbf{r}_1,\sigma_1)\phi_j^{e*}(\mathbf{r}_2,\sigma_2)\left(\frac{e^2}{4\pi\varepsilon\varepsilon_0|r_1-r_2|}\right)\phi_{i'}^{h*}((\mathbf{r}_1,\sigma_1))\phi_{j'}^e(\mathbf{r}_2,\sigma_2) \quad (8)$$

and exchange integrals

$$K_{ij,i'j'} = \sum_{\sigma_1\sigma_2} \iint d\mathbf{r}_1 d\mathbf{r}_2 \phi_i^h(\mathbf{r}_1,\sigma_1)\phi_j^{e*}(\mathbf{r}_2,\sigma_2)\left(\frac{e^2}{4\pi\varepsilon\varepsilon_0|r_1-r_2|}\right)\phi_{i'}^h(\mathbf{r}_2,\sigma_2)\phi_{j'}^e(\mathbf{r}_1,\sigma_1) \quad (9)$$

We use two hole and one electron single particle wave functions to build the excitons. We neglect band mixing[7-9] for the hole wave functions, restricting the hole basis to the two lowest states of the envelope function, 1S and 2S. The fine structure arising from spin-orbit coupling of the hole wave function and crystal field and exchange splitting[7-12] are neglected. The electron wave function is of 1S type. The radial densities of these wave functions are shown in Figure S2 for two QD radius.

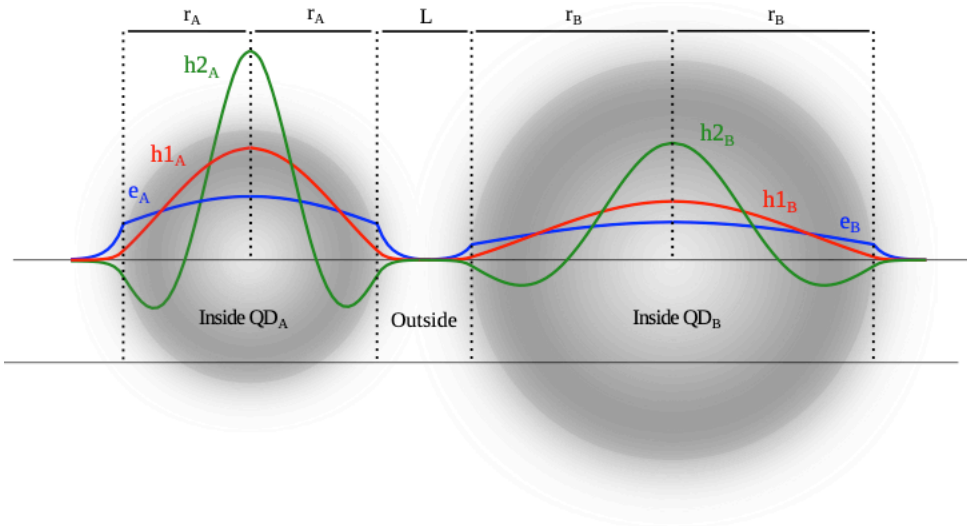

Figure S2 : Radial density the hole and electron wave functions for a heterodimer with r_A=1.175 and r_B=1.925 nm. The surface to surface distance, L is equal to 0.2 nm. The confinement effects are larger for the smaller size dot, QD_A, and for a given dot, larger for the electron and hole 2 wave functions than for hole 1.

3. Computation of the excitonic Coulomb integrals

The Coulomb couplings between different pairs of excitons are shown schematically in Figure S3.

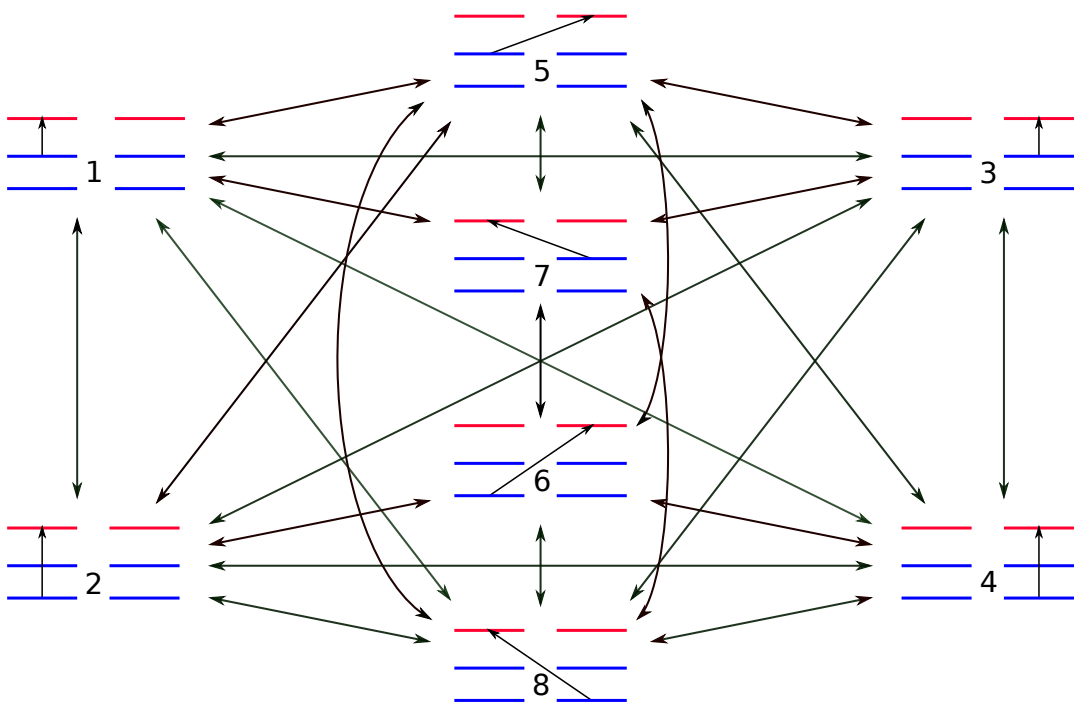

Figure S3 Scheme of the Coulomb couplings taking place between the eight excitons. The numbering is the same as in Figure 2 of the main text.

Each Coulomb matrix element is a polycentric 6 dimensional integral for which the one particle wave functions can be localized either on QD_A or QD_B. It is computed using an in-house implementation of a two level Monte-Carlo (MC) sampling, one for coordinate **r**, and for each sampled vector **r**, another sampling for coordinate **r'** in a parallelepiped box as shown in Figure S4 below. Due to the spherical shape of the QD and the leaking of the one particle state wavefunctions outside of the well as well as the quadratic growth of the number of points due to the two level MC sampling, the integration volume has been chosen large enough to ensure a proper sampling of the wavefunction delocalization outside the QD volume but small enough to minimize the computation time. The buffer distance b to the border of the box has been chosen equal to 0.5 nm and the number of points sampled for each level of the procedure is 100 000.

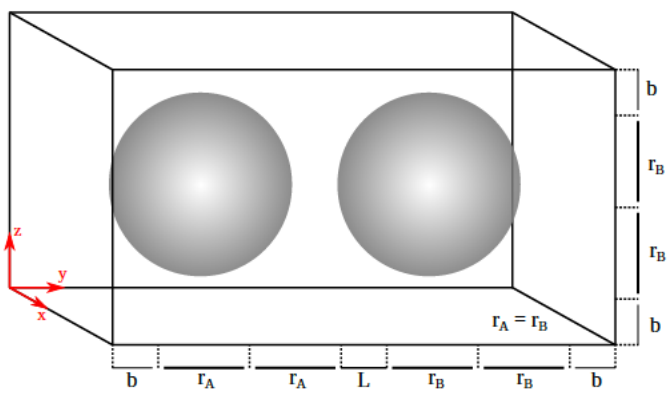

Figure S4 : Schematic representation of the integration volume used to compute the Coulomb matrix elements.

Since the integrated volume contains 3 distinct regions (namely inside QD_A, inside QD_B and outside of the QDs) and two position vectors, **r** and **r'**, must be sampled, it yields 9 different integration volumes in which the Coulomb integrals must be computed, as shown in Figure S5. Since there are two kinds of excitons (either local or CT), there are three types of exciton couplings (either local-local, local-CT, CT-CT). In the case of the coupling involving CT excitons, the contributions arising from the volume outside the QD, often neglected, are of utmost importance since they are responsible for a major part of the coupling strength. We do not separate short range and long range in the computation of the local-local Coulomb coupling matrix elements.

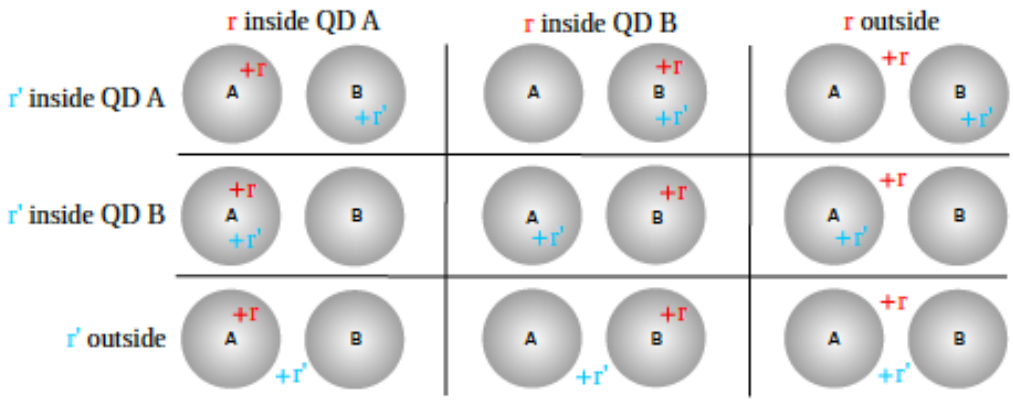

Figure S5. The 9 different integrations volumes used in the computation of the Coulomb integrals.

Both direct and exchange Coulomb integrals are systematically computed which gives rise to a set of 18 integrals for each exciton coupling of the model Hamiltonian. As an example, the full development of the integrals for the exciton coupling h1eA/h2B-eA is given below:

$$\mathbf{\Phi^{1-8}} = \langle \phi^A_{h1}(\mathbf{r})\phi^A_e(\mathbf{r}')|H_{e-h}|\phi^B_{h2}(\mathbf{r}-\mathbf{R})\phi^A_e(\mathbf{r}')\rangle$$

$$E^{inA/inA}_{eh} = \frac{A_{h1}(r_A)A^2_e(r_A)B_{h2}(r_B)e^2}{64\pi^3\epsilon_0}\times \int_r\int_{r'} \frac{sin(k^{h1}_{in}(r_A)|\mathbf{r}|)sin^2(k^e_{in}(r_A)|\mathbf{r}'|)exp(-k^{h2}_{out}(r_B)|\mathbf{r}-\mathbf{R}|)}{\sqrt{\epsilon_r(r_A,|\mathbf{r}-\mathbf{r}'|)\epsilon_r(r_B,|\mathbf{r}-\mathbf{r}'|)}|\mathbf{r}|\ |\mathbf{r}'|^2\ |\mathbf{r}-\mathbf{R}|\ |\mathbf{r}-\mathbf{r}'|}dr'dr$$

$$E^{inA/inB}_{eh} = \frac{A_{h1}(r_A)B^2_e(r_A)B_{h2}(r_B)e^2}{64\pi^3\epsilon_0}\times \int_r\int_{r'} \frac{sin(k^{h1}_{in}(r_A)|\mathbf{r}|)exp^2(-k^e_{out}(r_A)|\mathbf{r}'|)exp(-k^{h2}_{out}(r_B)|\mathbf{r}-\mathbf{R}|)}{\sqrt{\epsilon_r(r_A)\epsilon_r(r_B)}|\mathbf{r}|\ |\mathbf{r}'|^2\ |\mathbf{r}-\mathbf{R}|\ |\mathbf{r}-\mathbf{r}'|}dr'dr$$

$$E^{inA/out}_{eh} = \frac{A_{h1}(r_A)B^2_e(r_A)B_{h2}(r_B)e^2}{64\pi^3\epsilon_0}\times \int_r\int_{r'} \frac{sin(k^{h1}_{in}(r_A)|\mathbf{r}|)exp^2(-k^e_{out}(r_A)|\mathbf{r}'|)exp(-k^{h2}_{out}(r_B)|\mathbf{r}-\mathbf{R}|)}{\sqrt{\epsilon_r(r_A)\epsilon_r(r_B)}|\mathbf{r}|\ |\mathbf{r}'|^2\ |\mathbf{r}-\mathbf{R}|\ |\mathbf{r}-\mathbf{r}'|}dr'dr$$

$$E^{inB/inB}_{eh} = \frac{B_{h1}(r_A)B^2_e(r_A)A_{h2}(r_B)e^2}{64\pi^3\epsilon_0}\times \int_r\int_{r'} \frac{exp(-k^{h1}_{out}(r_A)|\mathbf{r}|)exp^2(-k^e_{out}(r_A)|\mathbf{r}'|)sin(k^{h2}_{in}(r_B)|\mathbf{r}-\mathbf{R}|)}{\sqrt{\epsilon_r(r_A,|\mathbf{r}-\mathbf{r}'|)\epsilon_r(r_B,|\mathbf{r}-\mathbf{r}'|)}|\mathbf{r}|\ |\mathbf{r}'|^2\ |\mathbf{r}-\mathbf{R}|\ |\mathbf{r}-\mathbf{r}'|}dr'dr$$

$$E^{inB/inA}_{eh} = \frac{B_{h1}(r_A)A^2_e(r_A)A_{h2}(r_B)e^2}{64\pi^3\epsilon_0}\times \int_r\int_{r'} \frac{exp(-k^{h1}_{out}(r_A)|\mathbf{r}|)sin^2(k^e_{in}(r_A)|\mathbf{r}'|)sin(k^{h2}_{in}(r_B)|\mathbf{r}-\mathbf{R}|)}{\sqrt{\epsilon_r(r_A)\epsilon_r(r_B)}|\mathbf{r}|\ |\mathbf{r}'|^2\ |\mathbf{r}-\mathbf{R}|\ |\mathbf{r}-\mathbf{r}'|}dr'dr$$

$$E^{inB/out}_{eh} = \frac{B_{h1}(r_A)B^2_e(r_A)A_{h2}(r_B)e^2}{64\pi^3\epsilon_0}\times \int_r\int_{r'} \frac{exp(-k^{h1}_{out}(r_A)|\mathbf{r}|)exp^2(-k^e_{out}(r_A)|\mathbf{r}'|)sin(k^{h2}_{in}(r_B)|\mathbf{r}-\mathbf{R}|)}{\sqrt{\epsilon_r(r_A)\epsilon_r(r_B)}|\mathbf{r}|\ |\mathbf{r}'|^2\ |\mathbf{r}-\mathbf{R}|\ |\mathbf{r}-\mathbf{r}'|}dr'dr$$

$$E^{out/inA}_{eh} = \frac{B_{h1}(r_A)A^2_e(r_A)B_{h2}(r_B)e^2}{64\pi^3\epsilon_0}\times \int_r\int_{r'} \frac{exp(-k^{h1}_{out}(r_A)|\mathbf{r}|)sin^2(k^e_{in}(r_A)|\mathbf{r}'|)exp(-k^{h2}_{out}(r_B)|\mathbf{r}-\mathbf{R}|)}{\sqrt{\epsilon_r(r_A)\epsilon_r(r_B)}|\mathbf{r}|\ |\mathbf{r}'|^2\ |\mathbf{r}-\mathbf{R}|\ |\mathbf{r}-\mathbf{r}'|}dr'dr$$

$$E_{eh}^{out/inB} = \frac{B_{h1}(r_A)B_e^2(r_A)B_{h2}(r_B)e^2}{64\pi^3\epsilon_0}\times$$
$$\int_r\int_{r'} \frac{exp(-k_{out}^{h1}(r_A)|\mathbf{r}|)exp^2(-k_{out}^{e}(r_A)|\mathbf{r}'|)exp(-k_{out}^{h2}(r_B)|\mathbf{r}-\mathbf{R}|)}{\sqrt{\epsilon_r(r_A)\epsilon_r(r_B)}|\mathbf{r}|\ |\mathbf{r}'|^2\ |\mathbf{r}-\mathbf{R}|\ |\mathbf{r}-\mathbf{r}'|}dr'dr$$

$$E_{eh}^{out/out} = \frac{B_{h1}(r_A)B_e^2(r_A)B_{h2}(r_B)e^2}{64\pi^3\epsilon_0}\times$$
$$\int_r\int_{r'} \frac{exp(-k_{out}^{h1}(r_A)|\mathbf{r}|)exp^2(-k_{out}^{e}(r_A)|\mathbf{r}'|)exp(-k_{out}^{h2}(r_B)|\mathbf{r}-\mathbf{R}|)}{\sqrt{\epsilon_r(r_A)\epsilon_r(r_B)}|\mathbf{r}|\ |\mathbf{r}'|^2\ |\mathbf{r}-\mathbf{R}|\ |\mathbf{r}-\mathbf{r}'|}dr'dr$$

$$\mathbf{\Phi_{Ex}^{1-8}} = \langle\phi_{h1}^A(\mathbf{r})\phi_e^A(\mathbf{r})|H_{e-h}|\phi_{h2}^B(\mathbf{r}'-\mathbf{R})\phi_e^A(\mathbf{r}')\rangle$$

$$E_{eh}^{inA/inA} = \frac{A_{h1}(r_A)A_e(r_A)B_{h2}(r_B)A_e(r_A)e^2}{64\pi^3\epsilon_0}\times$$
$$\int_r\int_{r'} \frac{sin(k_{in}^{h1}(r_A)|\mathbf{r}|)sin(k_{in}^{e}(r_A)|\mathbf{r}|)exp(-k_{out}^{h2}(r_B)|\mathbf{r}'-\mathbf{R}|)sin(k_{in}^{e}(r_A)|\mathbf{r}'|)}{\sqrt{\epsilon_r(r_A,|\mathbf{r}-\mathbf{r}'|)\epsilon_r(r_B,|\mathbf{r}-\mathbf{r}'|)}|\mathbf{r}|^2\ |\mathbf{r}'|^2\ |\mathbf{r}'-\mathbf{R}|\ |\mathbf{r}-\mathbf{r}'|}dr'dr$$

$$E_{eh}^{inA/inB} = \frac{A_{h1}(r_A)A_e(r_A)A_{h2}(r_B)B_e(r_A)e^2}{64\pi^3\epsilon_0}\times$$
$$\int_r\int_{r'} \frac{sin(k_{in}^{h1}(r_A)|\mathbf{r}|)sin(k_{in}^{e}(r_A)|\mathbf{r}|)sin(k_{in}^{h2}(r_B)|\mathbf{r}'-\mathbf{R}|)exp(-k_{out}^{e}(r_A)|\mathbf{r}'|)}{\sqrt{\epsilon_r(r_A)\epsilon_r(r_B)}|\mathbf{r}|^2\ |\mathbf{r}'|^2\ |\mathbf{r}'-\mathbf{R}|\ |\mathbf{r}-\mathbf{r}'|}dr'dr$$

$$E_{eh}^{inA/out} = \frac{A_{h1}(r_A)A_e(r_A)B_{h2}(r_B)B_e(r_A)e^2}{64\pi^3\epsilon_0}\times$$
$$\int_r\int_{r'} \frac{sin(k_{in}^{h1}(r_A)|\mathbf{r}|)sin(k_{in}^{e}(r_A)|\mathbf{r}|)exp(-k_{out}^{h2}(r_B)|\mathbf{r}'-\mathbf{R}|)exp(-k_{out}^{e}(r_A)|\mathbf{r}'|)}{\sqrt{\epsilon_r(r_A)\epsilon_r(r_B)}|\mathbf{r}|^2\ |\mathbf{r}'|^2\ |\mathbf{r}'-\mathbf{R}|\ |\mathbf{r}-\mathbf{r}'|}dr'dr$$

$$E_{eh}^{inB/inB} = \frac{B_{h1}(r_A)B_e(r_A)A_{h2}(r_B)B_e(r_A)e^2}{64\pi^3\epsilon_0}\times$$
$$\int_r\int_{r'} \frac{exp(-k_{out}^{h1}(r_A)|\mathbf{r}|)exp(-k_{out}^{e}(r_A)|\mathbf{r}|)sin(k_{in}^{h2}(r_B)|\mathbf{r}'-\mathbf{R}|)exp(-k_{out}^{e}(r_A)|\mathbf{r}'|)}{\sqrt{\epsilon_r(r_A,|\mathbf{r}-\mathbf{r}'|)\epsilon_r(r_B,|\mathbf{r}-\mathbf{r}'|)}|\mathbf{r}|^2\ |\mathbf{r}'|^2\ |\mathbf{r}'-\mathbf{R}|\ |\mathbf{r}-\mathbf{r}'|}dr'dr$$

$$E_{eh}^{inB/inA} = \frac{B_{h1}(r_A)B_e(r_A)B_{h2}(r_B)A_e(r_A)e^2}{64\pi^3\epsilon_0}\times$$
$$\int_r\int_{r'} \frac{exp(-k_{out}^{h1}(r_A)|\mathbf{r}|)exp(-k_{out}^{e}(r_A)|\mathbf{r}|)exp(-k_{out}^{h2}(r_B)|\mathbf{r}'-\mathbf{R}|)sin(k_{in}^{e}(r_A)|\mathbf{r}'|)}{\sqrt{\epsilon_r(r_A)\epsilon_r(r_B)}|\mathbf{r}|^2\ |\mathbf{r}'|^2\ |\mathbf{r}'-\mathbf{R}|\ |\mathbf{r}-\mathbf{r}'|}dr'dr$$

$$E_{eh}^{inB/out} = \frac{B_{h1}(r_A)B_e(r_A)B_{h2}(r_B)B_e(r_A)e^2}{64\pi^3\epsilon_0} \times$$
$$\int_r \int_{r'} \frac{exp(-k_{out}^{h1}(r_A)|\mathbf{r}|)exp(-k_{out}^{e}(r_A)|\mathbf{r}|)exp(-k_{out}^{h2}(r_B)|\mathbf{r}'-\mathbf{R}|)exp(-k_{out}^{e}(r_A)|\mathbf{r}'|)}{\sqrt{\epsilon_r(r_A)\epsilon_r(r_B)}|\mathbf{r}|^2\ |\mathbf{r}'|^2\ |\mathbf{r}'-\mathbf{R}|\ |\mathbf{r}-\mathbf{r}'|} dr'dr$$

$$E_{eh}^{out/inA} = \frac{B_{h1}(r_A)B_e(r_A)B_{h2}(r_B)A_e(r_A)e^2}{64\pi^3\epsilon_0} \times$$
$$\int_r \int_{r'} \frac{exp(-k_{out}^{h1}(r_A)|\mathbf{r}|)exp(-k_{out}^{e}(r_A)|\mathbf{r}|)exp(-k_{out}^{h2}(r_B)|\mathbf{r}'-\mathbf{R}|)sin(k_{in}^{e}(r_A)|\mathbf{r}'|)}{\sqrt{\epsilon_r(r_A)\epsilon_r(r_B)}|\mathbf{r}|^2\ |\mathbf{r}'|^2\ |\mathbf{r}'-\mathbf{R}|\ |\mathbf{r}-\mathbf{r}'|} dr'dr$$

$$E_{eh}^{out/inB} = \frac{B_{h1}(r_A)B_e(r_A)A_{h2}(r_B)B_e(r_A)e^2}{64\pi^3\epsilon_0} \times$$
$$\int_r \int_{r'} \frac{exp(-k_{out}^{h1}(r_A)|\mathbf{r}|)exp(-k_{out}^{e}(r_A)|\mathbf{r}|)sin(k_{in}^{h2}(r_B)|\mathbf{r}'-\mathbf{R}|)exp(-k_{out}^{e}(r_A)|\mathbf{r}'|)}{\sqrt{\epsilon_r(r_A)\epsilon_r(r_B)}|\mathbf{r}|^2\ |\mathbf{r}'|^2\ |\mathbf{r}'-\mathbf{R}|\ |\mathbf{r}-\mathbf{r}'|} dr'dr$$

$$E_{eh}^{out/out} = \frac{B_{h1}(r_A)B_e(r_A)B_{h2}(r_B)B_e(r_A)e^2}{64\pi^3\epsilon_0} \times$$
$$\int_r \int_{r'} \frac{exp(-k_{out}^{h1}(r_A)|\mathbf{r}|)exp(-k_{out}^{e}(r_A)|\mathbf{r}|)exp(-k_{out}^{h2}(r_B)|\mathbf{r}'-\mathbf{R}|)exp(-k_{out}^{e}(r_A)|\mathbf{r}|)}{\sqrt{\epsilon_r(r_A)\epsilon_r(r_B)}|\mathbf{r}|^2\ |\mathbf{r}'|^2\ |\mathbf{r}'-\mathbf{R}|\ |\mathbf{r}-\mathbf{r}'|} dr'dr$$

The Coulomb integrals have been screened by the dielectric constant of the material. This value is both dependent on the size of the QD, on the dielectric constant of the bulk material and on the particle to particle distance when both are found inside the same QD. The dependence of the dielectric constant on the QD radius *a* is taken as in ref. [13]

$$\varepsilon(a) = 1 + \frac{\varepsilon_0 - 1}{1 + \left(\frac{0.75\,10-9}{2a}\right)^{1.2}} \quad (10)$$

with the bulk dielectric constant ε_0 = 9.52. Taking into account the intradot particle to particle interaction, the dielectric constant inside a QD takes the form:

$$\frac{1}{\varepsilon(R,a)} = \frac{1}{\varepsilon(a)} - \left(\frac{1}{\varepsilon(a)} - \frac{1}{\varepsilon(a)+\Delta_{ion}}\right)\left(1 - \frac{\exp(-R/\rho_e) + \exp(-R/\rho_h)}{2}\right) \quad (11)$$

with

$$\rho_e = \left(2m_e^*\omega_{LO}/\hbar\right)^{-1/2} \text{ and } \rho_h = \left(2m_h^*\omega_{LO}/\hbar\right)^{-1/2} \quad (12)$$

$R = |r - r'|$ is the distance between the two particles, m_e^*= 0.13 m_e , m_h^*=0.82 m_e, Δ_{ion} = 3.5 is the screening parameter, ω_{LO} = 200 cm^{-1}. This value is shown as a function of the QD radius, *a,* in Figure S6 below for an average distance between the two particles in the QD over the sampling, *R*, equal to 35/36 *a*).

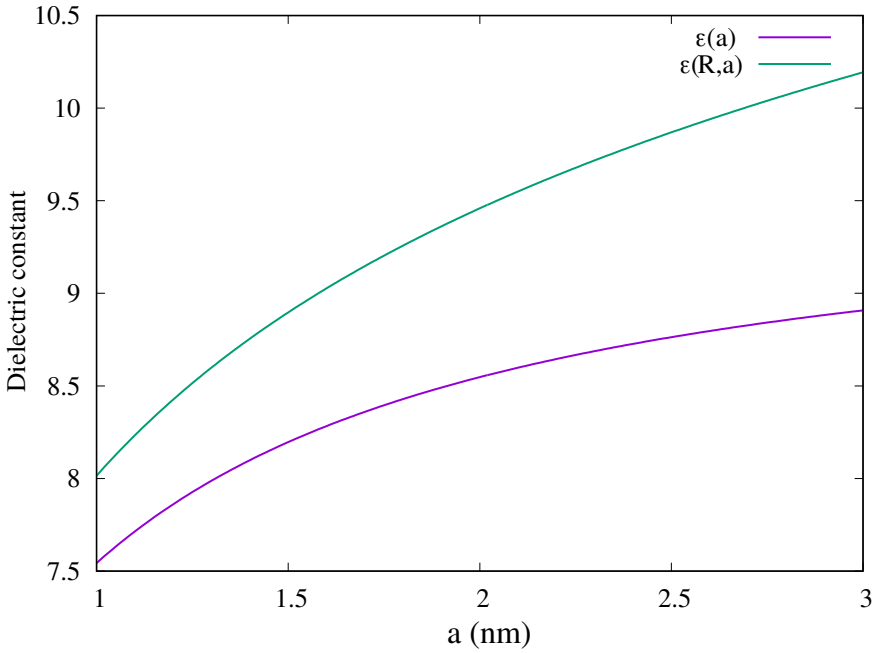

Figure S6. Dependence of the dielectric constant on the QD radius *a* for non interacting particles (violet), Eq. (10) and for interacting particles within the same QD volume (green), Eq.(11) with a value of *R* = 35/36 *a*

In addition, the value of the dielectric constant at a specific point in the integration box depends on the distance, *d*, from the center of the QD and is screened by the dielectric constant of the medium (considered here as organic ligands $\varepsilon_{out} = 2.3$). The expression used[13] is :

$$\varepsilon(d) = \varepsilon_{out} + \left(\varepsilon(a) - \varepsilon_{out}\right)\left(\frac{1}{2} - \frac{1}{\pi}\tan^{-1}\left(S(d-a)\right)\right) \qquad (13)$$

where $S = 5\ 10^9$ nm^{-1}. Figure S7 shows this dependence as a function of the distance from the center of the QD, *d*.

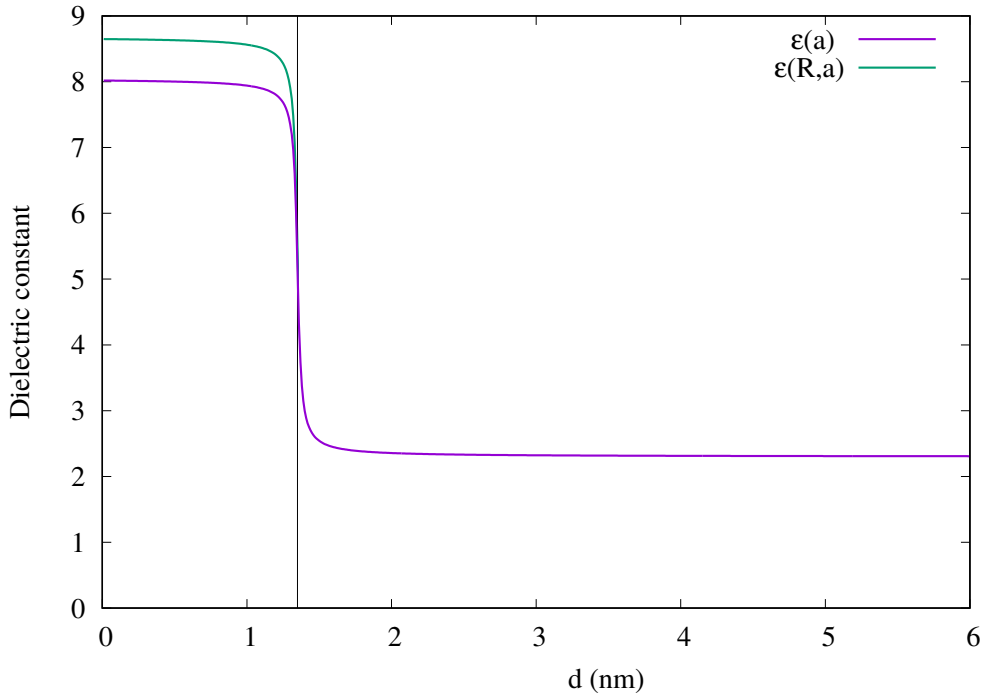

Figure S7. Dielectric function, Eq.(13) as a function of the distance, *d*, from the QD center for non-interacting particles (violet, Eq. (10)) and for interacting particles within the same QD volume (green, Eq.(11)).

The computed values of selected Coulomb matrix elements as a function of the sizes of QD_A and QD_B for a value of the surface to surface distance L=0.2nm are plotted in figure S8.

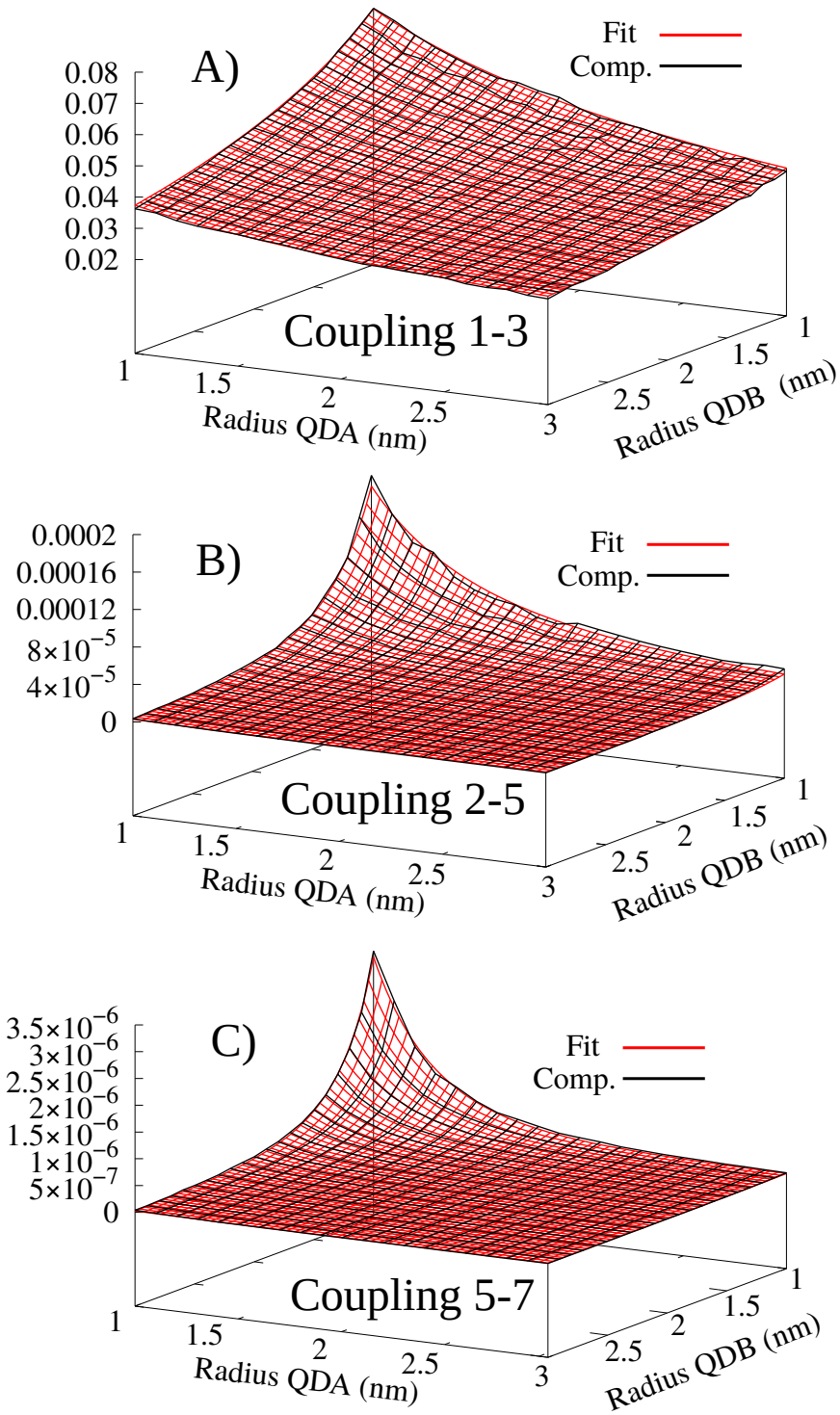

Figure S8. Dependence of the Coulomb matrix elements between excitons on the radius of QD_A and QD_B for a fixed surface to surface distance L=0.2 nm. Also shown is the fit used when sampling the sizes of 1000 dimers. The numbering and nature of the pair of excitons involved is given in Figure 2. The pair 1-3 (panel A) corresponds to the Coulomb coupling between two local excitons, $h1e_A$ and $h1e_B$. The pair 2-5 (panel B) corresponds to the Coulomb coupling between a local exciton (h2eA) and a CT exciton ($h1_A$-e_B). The pair 5-7 (panel C) corresponds to the Coulomb coupling between tow CT excitons, $h1_A$-e_B and $h1_B$-e_A. Note that

the Coulomb coupling decreases about 2 orders of magnitude when going from Local-Local to Local-CT and another 2 orders of magnitude from Local-CT to CT-CT. Note also that the dependence on the QD size is much stronger for the coupling terms that involve a CT exciton, because for a fixed L value, increasing the QD radius increases the center to center distance, R. The coupling between excitons that involve a CT state decrease exponentially as a function of R.

4. Computation of the transition dipole matrix elements

The transition dipoles are non zero for pairs of excitons that differ at most by a one particle wave function:

$$\mu_{kk'} = \int d\mathbf{r}\, \phi_{h/e}^{k}(\mathbf{r})\mathbf{r}\phi_{h/e}^{k'}(\mathbf{r}) \text{ where } k = 1,\ldots,8 \qquad (14)$$

The transition dipoles were computed numerically both from the GS and between excitons. Transition dipoles from the GS to exciton k with wave function $\phi_h^k \phi_e^k$ take the form

$$\mu_{GS-k} = \int d\mathbf{r}\, \phi_h^k(\mathbf{r})\mathbf{r}\phi_e^k(\mathbf{r}) \quad k = 1,\ldots,8 \qquad (15)$$

We give as an example the expression of the transition dipole matrix elements from the GS to a local exciton because they have an analytical expression:

$$\mu^{h-e} = e\int d\mathbf{r}\frac{A_e \sin\left(k_{in}^e \mathbf{r}\right) A_h \sin\left(k_{in}^h \mathbf{r}\right)}{4\pi\mathbf{r}} + e\int d\mathbf{r}\frac{B_e \sin\left(k_{in}^e \mathbf{r}\right) B_h \sin\left(k_{in}^h \mathbf{r}\right)}{4\pi\mathbf{r}} = \mu_{in}^{h-e} + \mu_{out}^{h-e} \quad (16)$$

where the first term corresponds to the volume inside the QD and the second to the volume outside the QD.

The term inside the dot is given by :

$$\mu_{in}^{h-e} = \int drA_e \sin\left(k_{in}^e r\right) A_h \sin\left(k_{in}^h r\right)$$

$$= \int_0^a dr\frac{A_e A_h}{2}\left(\frac{r\sin\left(r\left(k_{in}^e - k_{in}^h\right)\right)}{\left(k_{in}^e - k_{in}^h\right)} - \frac{r\sin\left(r\left(k_{in}^e + k_{in}^h\right)\right)}{\left(k_{in}^e + k_{in}^h\right)} + \frac{\cos\left(r\left(k_{in}^e - k_{in}^h\right)\right)}{\left(k_{in}^e - k_{in}^h\right)^2} - \frac{\cos\left(r\left(k_{in}^e + k_{in}^h\right)\right)}{\left(k_{in}^e + k_{in}^h\right)^2}\right)$$

(17)

$$\mu_{out}^{h-e} = \int drB_e \exp\left(-k_{out}^e r\right) B_h \exp\left(-k_{out}^h r\right)$$

$$= \int_a^{2a} drB_e B_h \frac{\exp\left(-r\left(k_{out}^e + k_{out}^h\right)\right)\left(r\left(k_{out}^e + k_{out}^h\right) + 1\right)}{\left(k_{out}^e + k_{out}^h\right)^2} \qquad (18)$$

Figure S9 shows the value of the local dipole transition moment for exciton h1e and h2e as a function of the dot radius, *a*.

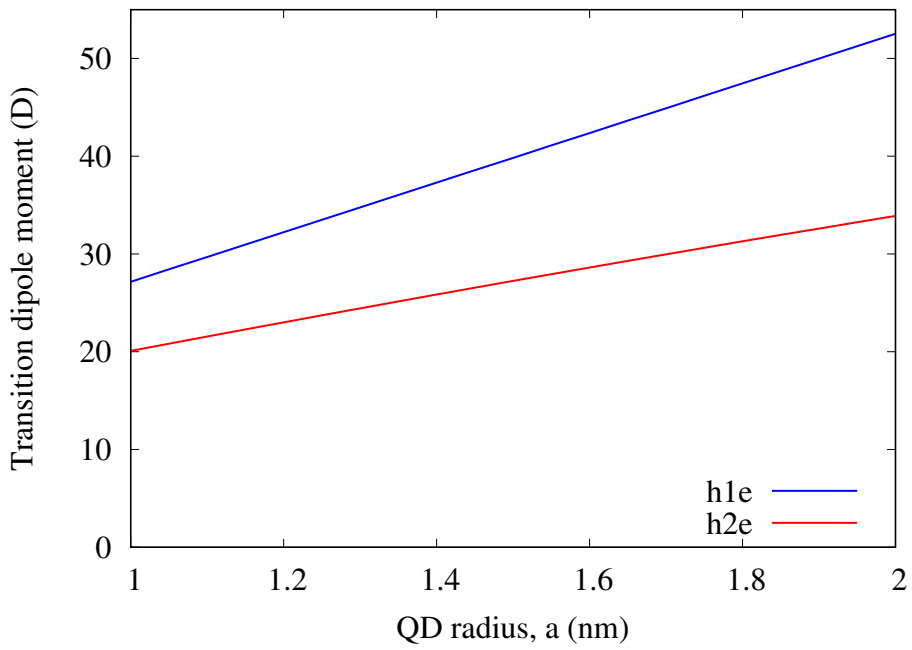

Figure S9. Computed value of the transition dipole to the local exciton h1e and h2e as function of the dot radius, *a*.

5. Dispersion of the electronic properties as a function of the ensemble of dimers

The size of each dot in the dimer is drawn from a Gaussian distribution, $D = \left(1/\sqrt{2\pi}\sigma\right)\exp\left(\left(D - D_{mean}\right)^2 / 2\sigma^2\right)$ with $\sigma = \%dis \times D_{mean}$. An example is shown in Figure S10 for the heterodimer discussed in the main text, with mean values of the diameters D_A = 2.25 nm and D_B=3.85 nm with 3% diameter dispersion in σ . In the case of the homodimer, one size distribution is used.

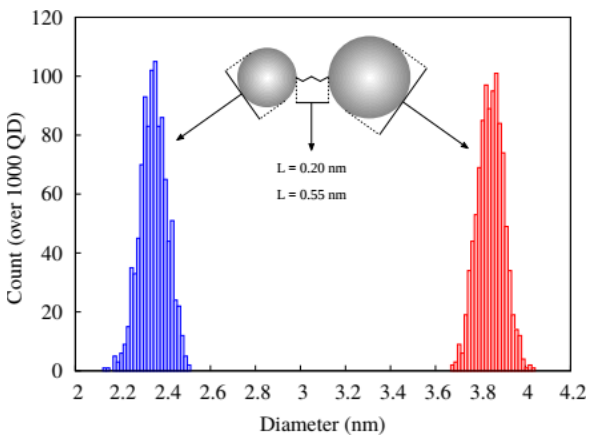

Figure S10 : Gaussian size distribution with 3% dispersion in diameter of the two QD A and B used to build the hetero dimer.

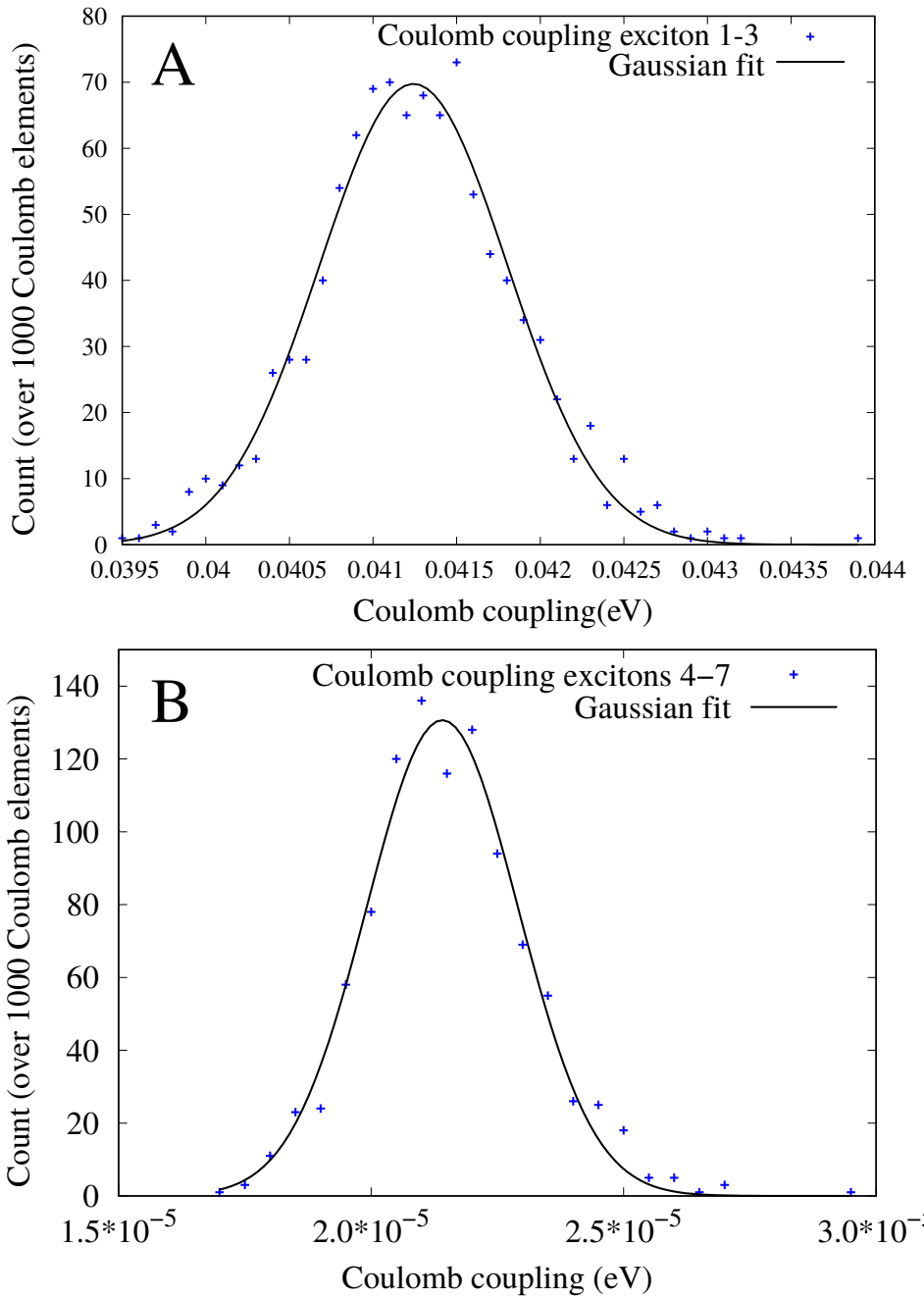

Figure S11 : Distribution of the Coulomb matrix elements in the dimer ensemble. Top: Local-local Coulomb coupling between excitons 1-3, bottom : local-CT coupling between excitons 4 and 7. The parameters of the Gaussian fits are given in Table S1.

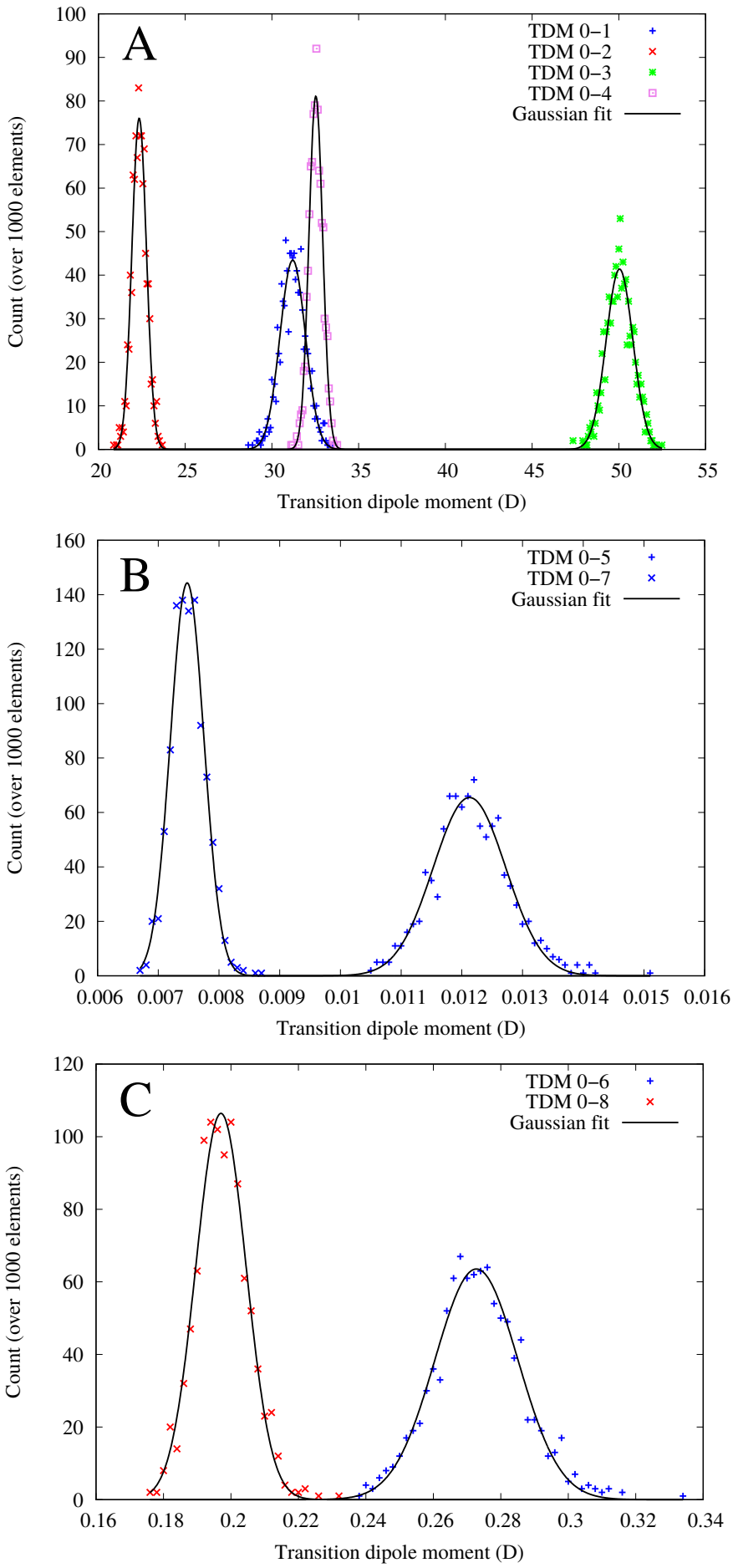
A
TDM 0–1
TDM 0–2
TDM 0–3
TDM 0–4
Gaussian fit
Count (over 1000 elements)
Transition dipole moment (D)
B
TDM 0–5
TDM 0–7
Gaussian fit
Count (over 1000 elements)
Transition dipole moment (D)
C
TDM 0–6
TDM 0–8
Gaussian fit
Count (over 1000 elements)
Transition dipole moment (D)

Figure S12. Distribution of the transition dipole matrix elements in the zero order exciton basis computed for the heterodimer of Figure 4A (mean diameter of QD_A=2.25 nm and mean diameter of QD_B = 3.85 nm , 3% size dispersion and L=0.2 nm). Top panel : the GS to local exciton dipole matrix elements, middle panel : GS to CT excitons 5 and 7, bottom panel : GS to CT excitons 6 and 8. The distributions are Gaussian, the parameters are given in Table S1.

Table S1 : parameters of the Gaussian fits for the zero order energies of Figure 4A, Coulomb matrix elements of Fig. S11 and transition dipole matrix elements of Fig. S12. Energies and the Gaussian width σ are given in eV.

$$F_{Gaussian}(x) = \frac{A}{\sigma\sqrt{2\pi}} \exp\left(\frac{-(x-\mu)^2}{2\sigma^2} \right)$$

Exciton energy	parameter	value	error	Error percentage
$h1e_A$	A	5.0076	0.0906	1.81%
	μ	2.1956	0.0002	0.01%
	σ	0.0104	0.0002	2.08%
h2eA	A	4.8922	0.1018	2.08%
	μ	2.3288	0.0003	0.01%
	σ	0.0133	0.0003	2.41%
h1eB	A	4.9156	0.1362	2.77%
	μ	2.4341	0.0005	0.02%
	σ	0.0150	0.0005	3.21%
h2eB	A	5.0112	0.0867	1.73%
	μ	2.4383	0.0004	0.02%
	σ	0.0191	0.0004	2.00%
h1A-eB	A	4.9742	0.1269	2.55%
	μ	2.6185	0.0008	0.03%
	σ	0.0271	0.0008	2.96%

h2A-eB	A	4.9300	0.1492	3.02%
	μ	2.7677	0.0007	0.02%
	σ	0.01926	0.0007	3.51%
h1A-eA	A	4.9451	0.1267	2.56%
	μ	3.1681	0.0015	0.05%
	σ	0.0496	0.0015	2.97%
h2B-eA	A	4.9690	0.1565	3.15%
	μ	3.3150	0.0022	0.07%
	σ	0.0618	0.0023	3.66%
Coulomb Matrix elements				
1-3	A	69.76	1.5	
	μ	0.0412	0.00001	
	σ	0.00056	0.00001	
4-7	A	130.66	3.89	
	μ	2.4e-5	5.1e-8	
	σ	1.5e-6	5.1e-8	
Transition matrix elements				
0-1	A	43.43	1.25	
	μ	31.200	0.024	
	σ	0.730	0.024	
0-2	A	76.04	1.87	
	μ	22.25	0.011	
	σ	0.417	0.011	
0-3	A	41.38	1.07	
	μ	50.04	0.023	
	σ	0.771	0.023	

0-4	A	81.10	1.61	
	μ	32.53	0.01	
	σ	0.394	0.01	
0-5	A	65.54	1.44	
	μ	0.012	0.00002	
	σ	0.0006	0.00002	
0-6	A	63.54	1.44	
	μ	0.273	0.0003	
	σ	0.012	0.0003	
0-7	A	144.32	4.078	
	μ	0.0075	9.0e-6	
	σ	0.00027	9.0e-6	
0-8	A	106.41	2.74	
	μ	0.197	0.00022	
	σ	0.0074	0.00022	

Section 6

Coherences involving eigenexcitons having large weights on local and CT states have a much smaller amplitude. Figure S13 shows representative examples of two local-CT electronic coherences computed for a specific heterodimer of the ensemble with mean sizes D_A= 2.7 nm and D_B = 3.5 nm whose level structure is shown in Figure 4B.

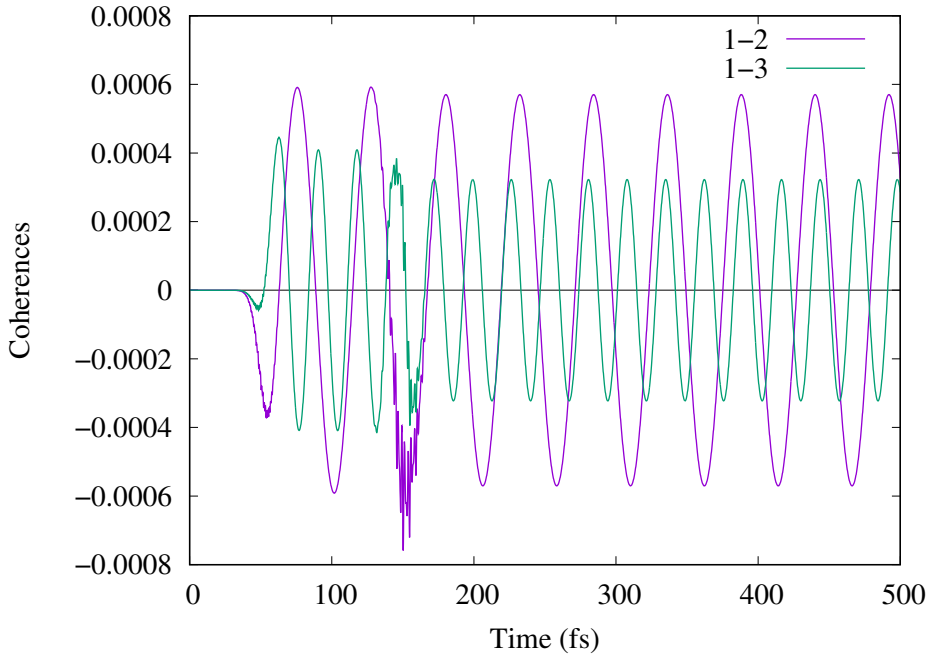

Figure S13. Dynamic of two local -CT exciton coherences computed for a single heterodimer (D_A= 2.7 nm and D_B = 3.5 nm, level structure shown in Figure 4B) upon excitation by a sequence of the UV and the IR pulse with a delay time of 100fs. The coherence 1-2 corresponds to eigenexcitons having their main weights on $h1e_B$ and $h1_Ae_B$ and the coherence 1-3 to $h1e_B$ and $h1_Ae_B$.

References

1.Ferreyra, J. M.; Proetto, C. R., Quantum size effects on excitonic Coulomb and exchange energies in finite-barrier semiconductor quantum dots. *Phys. Rev. B* 1999, 60, 10672-10675.
2.Jasieniak, J.; Califano, M.; Watkins, S. E., Size-Dependent Valence and Conduction Band-Edge Energies of Semiconductor Nanocrystals. *ACS Nano* 2011, 5, 5888-5902.
3.Inamdar, S. N.; Ingole, P. P.; Haram, S. K., Determination of Band Structure Parameters and the Quasi-Particle Gap of CdSe Quantum Dots by Cyclic Voltammetry. *ChemPhysChem* 2008, 9, 2574-2579.
4.Yu, W. W.; Qu, L.; Guo, W.; Peng, X., Experimental Determination of the Extinction Coefficient of CdTe, CdSe, and CdS Nanocrystals. *Chem. Mater.* 2003, 15, 2854-2860.
5.Franceschetti, A.; Fu, H.; Wang, L. W.; Zunger, A., Many-body pseudopotential theory of excitons in InP and CdSe quantum dots. *Phys. Rev. B* 1999, 60, 1819-1829.
6.Mlinar, V.; Zunger, A., Internal electronic structure and fine structure of multiexcitons in semiconductor quantum dots. *Phys. Rev. B* 2009, 80, 205311.

7.Efros, A. L.; Rosen, M., The electronic structure of semi-conducting nanocrystal. *Ann. rev. Mater. Sci.* 2000, 475-521.
8.Efros, A. L.; Rosen, M.; Kuno, M.; Nirmal, M.; Norris, D. J.; Bawendi, M., Band-edge exciton in quantum dots of semiconductors with a degenerate valence band: Dark and bright exciton states. *Phys. Rev. B* 1996, 54, 4843-4856.
9.Norris, D. J.; Bawendi, M. G., Measurement and assignment of the size-dependent optical spectrum in CdSe quantum dots. *Phys. Rev. B* 1996, 53, 16338-16346.
10.Fu, H.; Wang, L.-W.; Zunger, A., Excitonic exchange splitting in bulk semiconductors. *Phys. Rev. B* 1999, 59, 5568-5574.
11.Sercel, P. C.; Efros, A. L., Band-Edge Exciton in CdSe and Other II–VI and III–V Compound Semiconductor Nanocrystals − Revisited. *Nano Lett.* 2018, 18, 4061-4068.
12.Sercel, P. C.; Shabaev, A.; Efros, A. L., Photoluminescence Enhancement through Symmetry Breaking Induced by Defects in Nanocrystals. *Nano Lett.* 2017, 17, 4820-4830.
13.Wang, L.-W.; Zunger, A., Pseudopotential calculations of nanoscale CdSe quantum dots. *Phys. Rev. B* 1996, 53, 9579-9582.